Catalysis Science & Technology

ROYAL SOCIETY OF CHEMISTRY

PAPER

View Article Online
View Journal

Cite this: DOI: 10.1039/d5cy01501d

Photothermal flash light doping of strontium titanate photocatalyst nanoparticles

Melanie Johanning, [a] Wanderson O. Silva, [b] Anselm Dreher, [c] Paul Kant, [c] Mara Blöchlinger, [a] Arthur E. Bouchez, [a] Coral Felipe Gracia, [d] Hannah Johnson, [d] Roland Dittmeyer, [c] Mathieu Soutrenon [b] and Kevin Sivula *[a]

Rhodium and lanthanum co-doped strontium titanate (Rh,La:$SrTiO_3$) is a promising material for green hydrogen (H_2) production *via* heterogeneous photocatalytic (PC) water splitting. State-of-the-art Rh,La:$SrTiO_3$ nanoparticle photocatalysts mitigate charge recombination using an undoped core/doped shell structure. However, the typically-employed synthesis methods use high temperatures >1000 °C in a slow dopant diffusion process, which induces inhomogeneities, causes nanoparticle sintering, and limits material performance. In this work, we demonstrate a rapid flash light annealing (FLA) technique that affords suitable nanoparticle doping in only 7.5 seconds. FLA samples show a PC performance three times greater than conventional thermal doping, which we attribute to mitigated particle sintering and dopants incorporated closer to the surface. Moreover, the H_2 evolution rate under full spectrum simulated solar illumination increased by 50% compared to the undoped precursor nanoparticles. Finally, varying the flash parameters shows the tunability of the FLA process. The developed method paves the way for extending rapid doping by FLA to other powdered materials without the need for ion implantation.

Received 9th December 2025,
Accepted 21st April 2026

DOI: 10.1039/d5cy01501d

rsc.li/catalysis

Introduction

Heterogeneous photocatalysis is predicted to be the most economically attractive route for the global-scale production of green hydrogen (H_2) directly from solar energy, if the technology can meet a threshold performance of *ca.* 5% solar-to-hydrogen (STH) efficiency with years-long durability.[1,2] Despite significant progress in recent years,[3–7] reported systems with potential scalability and stability still fall below this threshold. Of the many materials investigated, strontium titanate ($SrTiO_3$) stands out as one of the most promising and most investigated material candidates.[5,8–14] $SrTiO_3$-based photocatalysts offer good chemical and thermal stability, tunable properties due to their perovskite structure, and relatively high abundance of the principle elements.[8,15] State-of-the-art aluminum-doped (Al:$SrTiO_3$) nanoparticles (NPs) have demonstrated both, stable performance for 1000 h, and an apparent quantum yield (AQY) of almost unity under UV light.[9,10] Moreover, the scalability of $SrTiO_3$-based photocatalysis has been demonstrated on the order of 100 m^2 using immobilized Al:$SrTiO_3$ NPs as photocatalyst sheets.[11] However, low solar light harvesting due to its relatively large electronic band gap (3.2 eV) limits the STH efficiency of Al:$SrTiO_3$ and only less than 1% of STH efficiency was achieved.[9]

To enhance solar light harvesting while also maintaining decent performance, a strategy of Rh doping together with additional n-type co-doping (La, Sb, or Bi) has recently emerged.[6,12,16–19] The co-dopants are crucial for stabilizing the photoactive Rh^{3+} state and thus to avoid the formation of Rh^{4+} recombination centers.[17–20] Z-scheme photocatalyst sheets with Rh,La-doped strontium titanate (Rh,La:$SrTiO_3$) and Mo-doped bismuth vanadate as H_2 and oxygen (O_2) evolution particles, respectively, have achieved significant STH efficiency of over 1%.[5] Moreover, Bi instead of La co-doping was found to reduce the generation of oxygen-vacancy defect states, leading to a demonstration of Rh,Bi:$SrTiO_3$ in a Z-scheme with 7.1% AQY under 420 nm illumination and thus outperforming Rh,La:$SrTiO_3$.[5,6,12]

Despite these promising demonstrations of Rh-doped $SrTiO_3$ for H_2 evolution, improving the quantum yield (QY) is still needed to realize PC systems with practical viability. This task represents a challenge that requires further fundamental understanding of the charge dynamics as well as tunable

[a] *Laboratory for Molecular Engineering of Optoelectronic Nanomaterials (LIMNO), Institute of Chemical Sciences and Engineering, EPFL, Lausanne CH-1015, Switzerland. E-mail: kevin.sivula@epfl.ch*
[b] *Institute of Systems Engineering, HES-SO Valais-Wallis, Sion CH-1950, Switzerland*
[c] *Institute for Micro Process Engineering (IMVT), Karlsruhe Institute of Technology (KIT), 76344 Eggenstein-Leopoldshafen, Germany*
[d] *Materials Engineering, Toyota Motor Europe, 1930 Zaventem, Belgium*

synthesis techniques to control the doping characteristics. Indeed, the best performing Rh,La and Rh,Bi:$SrTiO_3$ NPs feature an undoped core/doped shell structure.[5,6,12] It has been suggested that the enhanced visible light absorption (and thus charge carrier generation) in proximity to the NP/water interface as well as the highly crystalline precursor template are reasons for the improved performance of the core/shell structure over homogeneously doped NPs.[12] Moreover, the junction between doped and undoped $SrTiO_3$ is also expected to play a role based on studies on non-visible light absorbing dopants in other materials.[21–23] However, the conventional synthesis of core/shell co-doped $SrTiO_3$ involves a relatively slow diffusion-based process between pre-formed $SrTiO_3$ NPs and oxide precursors of the dopants at 1100 °C for several hours.[6,12] Processing of NPs at these conditions limits the control of dopant concentration profiles and is unavoidably accompanied by NP sintering, which reduces the available surface area for PC and therefore diminishes performance. Alternatives to the conventional solid-state processing *via* thermal annealing (TA) have so far been little explored in the literature for the synthesis of core/shell-doped $SrTiO_3$: only few reports are available on the hydrothermal synthesis of $SrTiO_3$ with La and Nb dopants in the shell.[24,25] A rapid doping technique to synthesize core/shell-doped Rh,La:$SrTiO_3$ could improve the PC performance by mitigating sintering and incorporating the dopants closer to the surface.

To realize such rapid doping, an attractive alternative to TA is photothermal heating, which reduces processing times because the sample is directly heated through the absorption of high-energy light irradiation.[26–29] Rapid processing methods for semiconductors by photothermal annealing have been developed in the past years to afford greater control over their electronic properties and/or shortened processing time.[26,28,30–35] For example, the sintering of metal oxides, a process that requires self-diffusion and typically several hours at temperatures above 1100 °C, can be now realized in seconds by photothermal annealing using Xe flash lamps and powerful blue LEDs.[27,36–38] The rapid formation of high temperatures using flash lamps was also employed to dope semiconductors (most commonly after ion implantation),[30,32,33,39] synthesize metal oxide thin films,[40,41] catalyst NPs,[42–44] and single atom catalysts.[45,46]

Among different methods for photothermal annealing, flash light annealing (FLA) appears as a suitable candidate to develop a rapid synthesis method for core/shell-doped Rh,La:$SrTiO_3$. Compared to rapid thermal annealing with halogen lamps, FLA is known to provide greater surface sensitivity (*i.e.*, less substrate heating) and allow smaller processing times.[26] Flash lamps also provide relatively homogeneous illumination over the processing area, while laser annealing provides very local heating.[26] The FLA technique therefore appears more suitable for homogeneous, rapid doping of a precursor spread over a cm^2-scale surface area. Moreover, the FLA technology is commercially available and was already demonstrated for continuous processing and various applications.[26,28,30,47]

Based on these advances, we hypothesized that the Rh,La-doping of $SrTiO_3$ can be realized in much shorter times by photothermal FLA, which should minimize the surface loss by sintering and incorporate the dopants closer to the surface than conventional TA.

Herein we demonstrate FLA on $SrTiO_3$ NPs for the first time, establishing it as promising processing technique for Rh and La co-doping and compare FLA to conventional and short-time TA. We find that materials prepared by FLA significantly outperformed various thermal references for sacrificial photocatalytic (PC) H_2 evolution and showed a 50% higher H_2 evolution rate under full spectrum simulated sunlight compared to an undoped precursor. We further demonstrate the crucial enablers, reproducibility, and tunability of the FLA process.

Results and discussion

The FLA process developed in this work yields undoped core/Rh,La-doped shell NPs within seconds using a commercial $SrTiO_3$ NP precursor impregnated with Rh and La salts. The synthesis process illustrated in Fig. 1 comprises the main steps of precursor preparation, coating on silicon (Si) substrates, FLA or TA, and powder collection (for details see SI section 1.1).

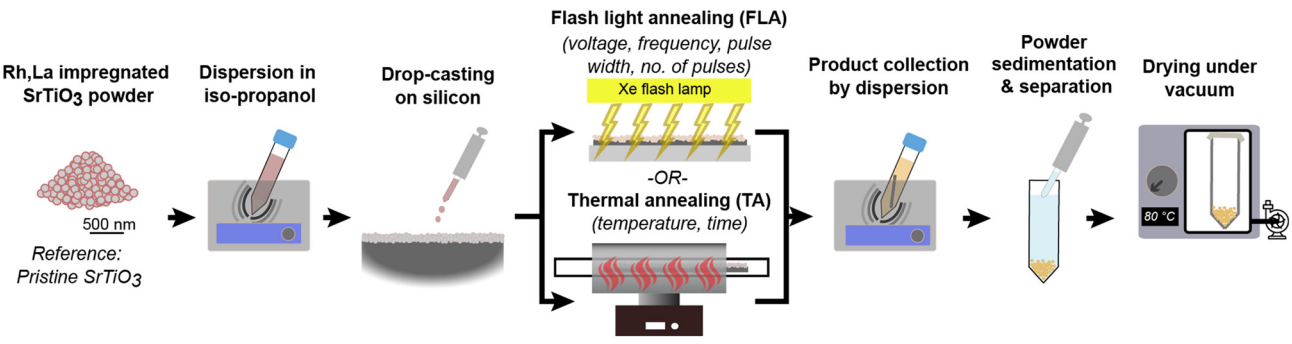

Fig. 1 Synthesis process to compare Rh,La-doping of commercial $SrTiO_3$ by flash light annealing (FLA) and thermal annealing (TA). Powders were coated on Si substrate for the annealing unless it is indicated that free powder was annealed directly. Undoped powder was coated and annealed in a similar manner as a reference.

In a typical synthesis, commercial $SrTiO_3$ NPs were impregnated with 1 at% Rh and La (based on Ti and Sr, respectively) from salts by wet grinding. Wet grinding does not change the particle size or shape (see Fig. S1 in SI) but presumably results in a more homogeneous coating with the water-soluble dopant precursors than dry grinding. The impregnated precursor or the pristine commercial precursor (as a control) were dispersed in isopropanol for coating on Si substrates before either FLA or TA. We note that 1 at% doping was chosen to limit the segregation of excess dopant precursors while drying the coated films. A loading of 3.2 mg cm^{-2} of the powder was coated on the substrate to enable homogeneous heating throughout the film (see scanning electron microscopy (SEM) images in Fig. S2 confirming a homogeneous transformation). After thermal treatment, the annealed samples were collected in water by sonication, separated by sedimentation, and dried to obtain a powder sample. FLA conditions were a pulse frequency of 60 Hz and pulse width of 1.5 ms for all samples. The voltage used to drive the flash lamp controls the light intensity and voltages of 225, 250, and 275 V were used. In addition, the number of pulses incident on each sample was varied between 450 and 7200. For details regarding the lamp energy consumption at each of the employed conditions, see Table S1. As a control, TA was performed at 1100 °C either in a muffle furnace for 6 h (3.6 h ramp time) or by introducing the sample into a pre-heated tube furnace (for times between 10 min and 120 min). We note that TA was also performed on free powder samples (not coated on Si substrates) in alumina crucibles. This applies to samples with labels including "powder" in the following discussion. Photographs of all samples after FLA and TA are shown in Fig. S3. The samples were examined for phase purity, optical absorption, morphology, particle size, elemental composition, surface dopant concentration, and PC performance (for experimental details, see SI section 1.2).

Doping by flash light annealing (FLA)

The powder transformation upon FLA is shown in Fig. 2 for an annealing time of 7.5 s (275 V and 450 pulses). The inset

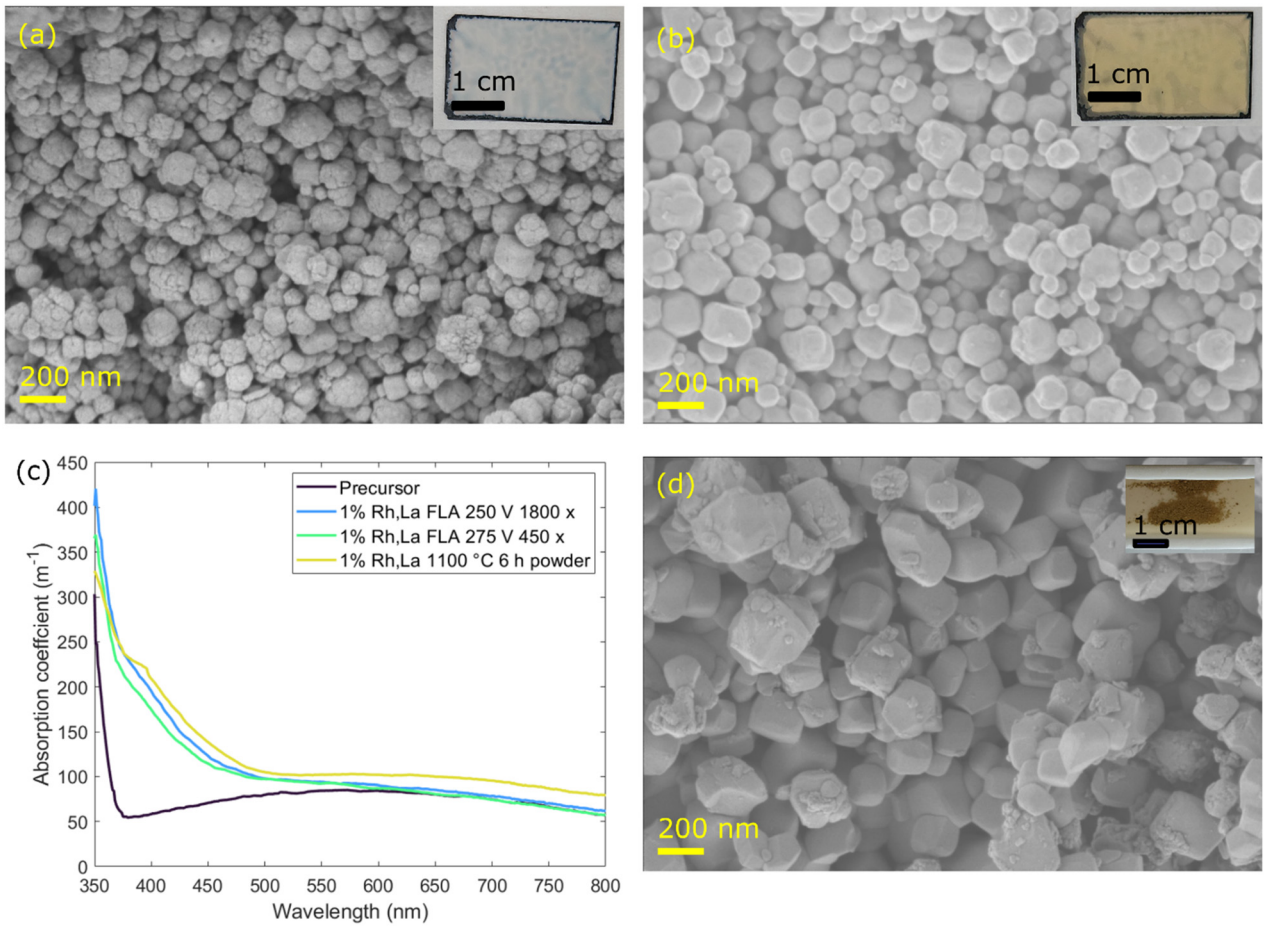

Fig. 2 SEM images and photograph inserts of the (a) Rh,La-impregnated $SrTiO_3$ precursor and (b) Rh,La:$SrTiO_3$ with restructured NP surface after FLA at 275 V for 450 pulses (7.5 s processing). (c) Optical absorption coefficients of powder dispersions (0.5 mg mL^{-1} in H_2O) comparing the undoped precursor, FLA doping at two conditions, and conventional doping by TA at 1100 °C for 6 h. (d) SEM image and photograph insert of Rh,La:$SrTiO_3$ doped by TA at 1100 °C for 6 h.

photographs in Fig. 2 show a clear color change of the Rh,La-impregnated, pale pink precursor in Fig. 2a into the yellow product in Fig. 2b. The yellow color of the product is characteristic for Rh,La:$SrTiO_3$ and thus a first indication for a successful doping.[12,19] The results of elemental analysis by inductively coupled plasma mass spectroscopy (ICP-MS) confirm the presence of Rh and La at the expected concentrations (see Table S2). Further, the presence of Si in the powder was not detected, which thus excludes unintended Si doping above the detection limit.

For measuring the change in optical properties, the optical absorption coefficients of dispersions were extracted from reflectance and transmittance measurements using a ray tracing optical model of the employed UV-vis cuvette (see SI section 1.2 for experimental details and Fig. S4 for the employed simulation geometry and resulting "optical behaviour map").[48–50] This method allows measuring the optical properties for a few mg of sample, which is beneficial for the small batch size of ~20 mg in this study. A conventional measurement of the Kubelka–Munk function would require around 100 mg of powder. The absorption coefficients in Fig. 2c show a clear shift of the absorption edge of undoped powder (*ca.* 375 nm) towards 500 nm after doping by two FLA conditions (for scattering coefficients, standard deviations, and raw data of transmission and reflection, see Fig. S5a and b). The absorption onset of around 500 nm after FLA matches well with the reported value for Rh^{3+} in Rh,La:$SrTiO_3$ (ref. 12) and the Kubelka–Munk function obtained from a diffuse reflectance measurement of a thermally doped reference (see Fig. S5c). An incorporation of only Rh would increase the absorption between 550 and 600 nm due to Rh^{4+} mid gap states.[12,19,20] The absence of this feature suggests the successful co-doping with both Rh and La.

The SEM images in Fig. 2 show a change in the particle morphology after FLA. The impregnated precursor in Fig. 2a has a rough particle surface. After FLA, the particle surface is smoother but the size and spherical shape appear to be mostly conserved (see Fig. 2b). X-ray diffraction (XRD) patterns confirm that the cubic perovskite structure of the precursor is maintained and no phase transformation occurred (see Fig. S6 for XRD patterns of all samples). Therefore, the morphology change is assigned to a surface restructuring of the rough particles upon annealing resulting from a high driving force to reduce their surface area. The essential role of this rapid surface restructuring for the doping by FLA is described later in the section on "process control".

Reference samples were produced by FLA and TA of the undoped precursor as well as Rh,La-doping through TA (for photographs and SEM images see Fig. S3, S7 and S8, respectively). Conventionally, Rh,La-doping is performed as a powder by TA at 1100 °C for 6 h plus an additional ramping time.[12] The sample annealed at these conditions has a similar yellow color and a comparable optical absorption coefficient as FLA samples (see Fig. 2c and d). This further supports the successful doping by FLA. The morphology change of the sample doped by TA for 6 h in Fig. 2d is however much more pronounced. The powder went through significant sintering and a remarkable change of the particle shape.

In an attempt to better compare TA to FLA, reference samples were also produced by TA at much shorter annealing times by sliding the samples coated on Si or as free powder in and out of a pre-heated tube furnace. The heating of an alumina crucible from room temperature to 1100 °C was estimated to take at least 5 min by measurements with a K-type thermocouple (see Fig. S9). Therefore, a minimum annealing time of 10 min by TA was chosen to allow a reproducible synthesis. These "fastest TA" conditions were then compared to FLA. The same characteristic color change is observed with TA for 10 min at 1100 °C (see Fig. S3). However, even at 10 min annealing time, more sintering and change in the particle morphology is observed when compared to FLA (see SEM images in Fig. S7). Undoped annealed reference samples show similar morphology changes as their corresponding doped samples from FLA and TA but no color change (see Fig. S3 and S8 for photographs and SEM images, respectively).

The spatial dopant distribution as undoped core/doped shell NPs has been reported as enabler of a good performance of Rh-doped $SrTiO_3$.[6,12] The dopant distribution in the spherical particles cannot be observed directly by mapping with scanning transmission electron microscopy with energy-dispersive X-ray spectroscopy (STEM-EDX) for the concentration of 1 at% due to an insufficient signal-to-noise ratio (see Fig. S10 for elemental maps after FLA and TA, line profile, and EDX spectrum). No overall increase of the net count rate for dopants is detected in the particle shell. However, the dopant distribution can be observed by STEM-EDX for 4 at% doping (see Fig. S11). In this case, STEM-EDX maps clearly show a shell enriched with Rh and La. While the rough surface restructured into a smooth surface, the internal particle structure featuring voids remained unchanged. This observation is similar to the FLA and TA samples with 1 at% doping (see Fig. S10). Thus, the FLA and TA samples with 1 at% doping are also expected to have a similar core/shell structure with doping most likely limited to the surface region. Nevertheless, the dopant depth profile may depend on the annealing time and method. The dopant distribution was thus qualitatively assessed in Fig. 3a by comparing the bulk concentration from ICP-MS and the surface concentration from X-ray photoelectron spectroscopy (XPS) as the share of all four elements Sr, Ti, Rh, and La (for XPS spectra with integration regions, see Fig. S12). The bulk dopant concentration remains within the error of measurement at the expected 0.5 at% after FLA or TA (0.5 at% as share of four elements). The dopants adsorbed to the surface of the impregnated precursor hence remain in the powder products. In contrast, the surface concentration from XPS is significantly higher after FLA than for the two samples annealed at 1100 °C for 10 min and 6 h. The dopants are thus present in higher concentration at the surface after FLA, which implies a thinner doped shell with higher dopant

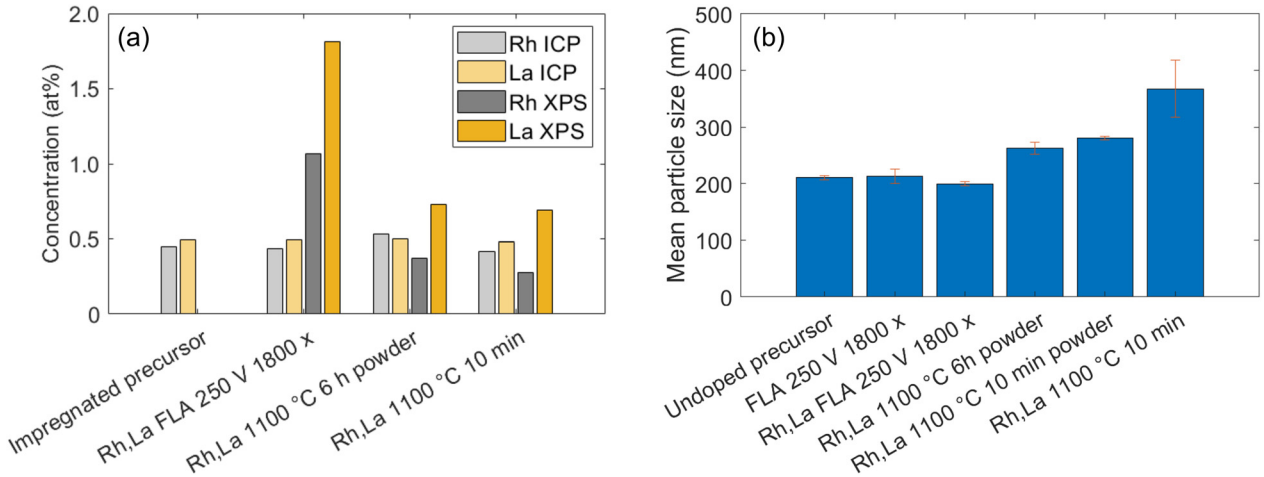

Fig. 3 (a) Bulk (ICP-MS) and surface (XPS) dopant concentrations for the impregnated precursor, after FLA at 250 V for 1800 pulses, and thermal references doped as powder at 1100 °C for 6 h and film at 1100 °C for 10 min. (b) Mean particle sizes and standard deviations obtained from number distributions based on DLS measurements of dispersions for the undoped precursor, undoped and doped samples from FLA and thermal references annealed as powder and film.

concentration. A second XPS measurement series on the same samples generally supports the same trend when comparing the different annealing techniques (see Fig. S12h). The Rh-to-La ratios extracted from this second XPS data set differ from the ones in Fig. 3b. These differences may arise from local fluctuations in the sample composition or experimental errors of the quantification *via* XPS. Quantification of Rh and La from XPS measurements on six different samples show comparable dopant concentrations and ratios close to 1 : 1 (see section "process control"). This suggests the different doping ratios in the case of Fig. 3a and S12h are most likely caused by local fluctuations of the dopant concentrations in the particular sample.

The incorporation of the dopants closer to the surface for FLA is further supported by the surface morphology of FLA and TA samples described above. After FLA, the powder retains a morphology with particle sizes and shapes very similar to the initial precursor. In contrast, thermally annealed samples show more significant changes in the morphology by more advanced surface restructuring and fusion of particles by sintering. This is expected to incorporate the dopants into a thicker shell at lower concentrations.

The morphological changes during TA also affect the particle size and thus available surface area for PC. The mean particle sizes were determined from dynamic light scattering (DLS) to provide a qualitative comparison of FLA and TA. Fig. 3b shows that the mean particle size for doped and undoped FLA particles remains comparable to the precursor (see Fig. S13 for particle size distributions). The particle size increases during TA, most significantly for the sample annealed as a film. This is assigned to the larger extent of sintering of individual particles into agglomerates when sintered as a coated film (see SEM images in Fig. S7). The size distribution is therefore broadened as well. As a reference, the size distributions were also analyzed by counting at least 200 particles in STEM images. The results in Fig. S14 support the general trend that FLA closely conserves the particle size and prevents sintering, while the particle size increases significantly during TA due to sintering. Furthermore, the trends in the particle size are also consistent with changes in the optical scattering coefficients of the dispersions. The scattering behavior depends on the ratio of the particle size and wavelength.[51] While the trend of the scattering coefficient remains closer to the pristine precursor for FLA samples, samples from TA show decreased scattering coefficients at shorter wavelengths (see Fig. S5a).

Overall, the developed FLA process successfully synthesized undoped core/doped shell Rh,La:$SrTiO_3$ with a morphology closer to the initial powder than for TA and incorporates the dopants closer to the particle surface. In parallel to the dopant incorporation, a surface restructuring was observed. The magnitude of morphology changes correlates well with the differences in dopant surface concentrations and is thus assumed to play a crucial mechanistic role for the dopant incorporation (see section "process control" for further investigation).

Photocatalytic performance of FLA compared to TA

The H_2 evolution rates in Fig. 4a compare the performance of doped and undoped $SrTiO_3$ prepared with FLA or TA (for details on PC testing methods, see section 1.2 in SI). Notably, testing was performed with the addition of a sacrificial electron donor (ascorbic acid) since Rh,La:$SrTiO_3$ cannot effectively oxidize water, and a Pt co-catalyst was used to facilitate the H_2 evolution reaction. The reproducibility of the PC testing and FLA process is demonstrated below (see section "process control"). Deviations of the H_2 evolution

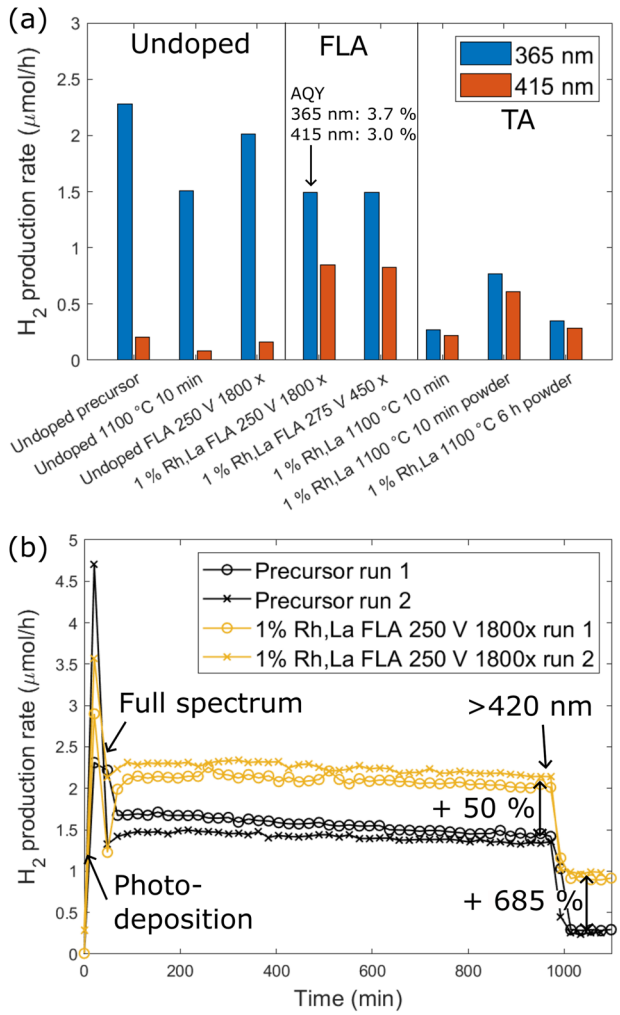

Fig. 4 PC performance of Rh,La:$SrTiO_3$ doped with the FLA and TA route along with undoped references. (a) Average performance under 365 and 415 nm illumination for undoped reference samples, 1 at% Rh,La-doped samples from FLA, and various thermal references (0.4 wt% Pt, 0.2 M ascorbic acid, average from 2 runs). (b) Full spectrum PC performance and stability test after *in situ* photodeposition at 365 nm. A 420 nm cut-off filter was introduced during the measurement.

rates for the FLA-prepared Rh,La:$SrTiO_3$ (at 250 V and 1800 pulses) are shown to be ±15%. These deviations are significantly lower than the differences measured between samples prepared with FLA or TA, as discussed below. The H_2 evolution rates in Fig. 4a were measured by a screening approach which does not allow accurate AQY measurements. As a benchmark, the performance of the FLA-prepared Rh,La:$SrTiO_3$ (250 V and 1800 pulses) corresponds to an AQY of 3.7% at 365 nm and 3.0% at 415 nm (for raw data and experimental details, see Fig. S15 and section 1.2 in the SI, respectively).

Rh,La:$SrTiO_3$ prepared by FLA at two conditions was found to outperform Rh,La:$SrTiO_3$ prepared by TA (either as coated films or as loose powder) at various representative conditions (see Fig. 4a and S16 for more conditions). The listed samples doped with FLA represent those with the best performances among all tested FLA conditions. The best performance for TA-prepared samples was achieved for powders annealed without the Si substrate in a pre-heated tube furnace for 10 min annealing time.

All undoped $SrTiO_3$ powders evolve H_2 under 365 nm illumination but only trace H_2 is detected at 415 nm due to the very limited light absorption at the latter wavelength. We cannot discount that the small H_2 production under 415 nm illumination in this case originates from a small number of photons with sufficient energy to excite undoped $SrTiO_3$ (for illumination spectral distributions, see Fig. S17a). The significantly increased H_2 evolution of Rh,La:$SrTiO_3$ at 415 nm confirms the successful doping when using the FLA or TA preparation routes. Processing *via* FLA reduced the H_2 evolution rate at 365 nm only slightly, but TA reduced the UV light performance more significantly. Samples from FLA therefore have a higher ratio of UV to visible light performance than for TA. Testing under full spectrum simulated solar illumination further emphasizes the difference between the FLA-treated and undoped samples. Here the FLA-prepared Rh,La:$SrTiO_3$ outperforms the undoped precursor $SrTiO_3$ by 50% and exhibits decent stability (see Fig. 4b). After removing photons with a wavelength below 420 nm from the illumination spectrum with a cut-off filter, the performance is 685% higher for the doped *vs.* the undoped sample (for illumination spectra, see Fig. S17b). To estimate the performance under standardized solar irradiance, the STH efficiency was calculated considering the spectral mismatch between the full spectrum emission from the Xe arc-lamp based solar simulator and the AM 1.5G standard spectrum with respect to the two different band gaps of the doped and undoped $SrTiO_3$ (for details see SI section 1.2). Applying this correction, a comparable STH performance of 0.11% for the undoped precursor and 0.12% for FLA-prepared Rh,La:$SrTiO_3$ was estimated. These results highlight the necessity for a comparison of undoped and doped samples under full spectrum illumination and taking into account the spectral mismatch rather than solely comparing the performance under visible light illumination.

The potential reasons for the higher H_2 evolution rates of the FLA-prepared samples compared to all samples doped by TA are discussed in the following. The PC performance data indicate a benefit of doping through FLA within shorter time beyond minimizing the loss of surface area. The different ratios of UV to visible light performance of the Rh,La:$SrTiO_3$ prepared with the FLA and TA approaches imply a different factor limiting their performances. If a loss of specific surface area (due to increased particle size of samples prepared by TA) was the sole factor to explain the performance differences, a similar performance loss would be expected for the undoped $SrTiO_3$ control sample after TA. This is not the case. Thus, we infer that the photogenerated charge recombination rate in TA-prepared Rh,La:$SrTiO_3$ is higher than for FLA-prepared samples for other reasons.

To evaluate if differences in the crystallinity are the origin of the different PC performance, we analyzed the crystallinity of three key samples by TEM. Note that the extraction of a crystal correlation length from XRD patterns is not reliable due to the small amount of powder measured in Bragg–Brentano geometry. Therefore, we used convergent-beam electron diffraction (CBED) and HRTEM to compare particles of the undoped $SrTiO_3$ precursor with Rh,La:$SrTiO_3$ prepared *via* FLA (250 V and 1800 pulses) and TA (1100 °C for 6 h). The results in Fig. S18 indicate the presence of only one crystal orientation in the particles of all three samples. The pristine precursor however shows a mesocrystal structure. As the morphology changes upon annealing, the composing sub-particles appear to fuse continuously with prolonged annealing (see above and SEM images in Fig. 2 and S7). This morphology change is more pronounced after TA than FLA. We thus exclude superior crystallinity as the origin of a better PC performance for FLA-doped Rh,La:$SrTiO_3$.

The valence and conduction band position of a semiconductor can affect its PC activity. The optical properties for FLA- and TA-prepared Rh,La:$SrTiO_3$ agree well with the reported absorption edges for Rh^{3+} doping of $SrTiO_3$ in the literature (see Fig. 2c).[12,19,20] Previous studies have investigated the band structure of Rh,La:$SrTiO_3$.[19,52] We expect similar electronic structures for our samples and no significant differences in the band edges for FLA- and TA-prepared samples due to their similar light absorption properties (see Fig. 2c). It is nevertheless possible that the concentration of defects (*e.g.*, oxygen vacancies) formed during doping depends on the annealing time and method. It was previously reported that Sr-rich phases incl. SrO_x segregate on the surface of undoped and doped $SrTiO_3$ single crystals during thermal annealing in oxidative atmospheres.[53–55] Such changes may affect the chemical composition on the surface and thus PC activity. While the quality of the XPS spectra on the powder does not allow a conclusive analysis due to issues with partial charging, it is possible to quantify the Sr/Ti-ratios on the surface. The results in Fig. S19 show that undoped $SrTiO_3$ and Rh,La:$SrTiO_3$ show a Sr excess after TA but the ratio remains close to 1 : 1 after FLA. This may suggest a different doping mechanism during the rapid FLA that kinetically inhibits the segregation of Sr on the surface. We note that our analysis of the crystallinity through TEM (see above) could not find any evidence for secondary phases in a Rh,La:$SrTiO_3$ particle after TA (1100 °C for 6 h). This factor thus needs further investigation in future studies to clarify the effect of the different processing time scales on the surface composition and defects of Rh,La:$SrTiO_3$ NPs.

As another factor, the incorporation of dopants closer to the surface by FLA may affect the PC properties by changing the thickness and composition of the doped shell. The effect of the core/shell structure on the PC performance of Rh-doped based $SrTiO_3$ is a topic of ongoing research.[6,12,56] The initial study on Rh,La:$SrTiO_3$ reported that the PC performance depends on the annealing time and assigned this to the evolving dopant distribution.[12] A recent study on Rh,Bi:$SrTiO_3$ found that a homogeneously doped sample showed a 10 times lower H_2 production rate than core/shell-doped particles.[6] Studies that control the shell thickness and dopant concentration independent from each other and other properties such as the particle morphology as well as in-depth mechanistic studies are still needed. Such systematic studies have been performed on other metal oxide photocatalysts with core/shell-doping of non-visible light absorbing dopants and found effects of the depth-dependent electronic structure on the charge separation.[21–23]

Based on our findings, (i) significant differences in the powder morphology and (ii) spatial dopant distribution between FLA and TA samples likely contribute to the superior PC performance of Rh,La:$SrTiO_3$ prepared from FLA. (i) Mitigated sintering during FLA, which is associated with a smaller particle size, increases the specific surface area available for the PC reaction, and may thus enhance the H_2 production rate. (ii) A thinner shell brings the visible light absorption, *i.e.*, carrier generation, closer to the particle surface.[12] In addition, if the thickness of the doped shell is reduced, this may allow more UV light to penetrate into the undoped regions effectively shortening the required diffusion length through the doped material (which possesses higher recombination rates). We speculate that these factors allow more charge carriers generated by UV light to reach the surface before recombination. Further, the interplay of the doped-undoped junction may be affected by changing the dopant distribution. Detailed investigations to understand the charge carrier dynamics in core/shell particles of Rh,La:$SrTiO_3$ are therefore necessary in future work.

Process control

The reproducibility of the FLA treatment was evaluated by analyzing six different samples of Rh,La:$SrTiO_3$ prepared at 250 V and 1800 pulses from the same precursor powder. The results are summarized in Fig. S20 (for photographs see Fig. S3). All samples have comparable powder morphology (see Fig. S20a–f), which is also similar to samples obtained from another precursor (in Fig. S2 and S7). The absorption and scattering coefficients of the sample dispersions (as shown in Fig. S20g and h) confirm comparable optical properties for the six samples, which are also in good agreement with optical properties obtained from processing a different precursor (Fig. 2c). The surface dopant concentrations (Fig. S20i) vary only slightly within an expected range (up to ±0.5 at%) and are comparable to the sample presented in Fig. 3a. The Rh-to-La ratio for these samples is close to 1 : 1. The PC performance of eight samples from three different precursors is shown in Fig. S20j. The average H_2 production rate of all measurements is 1.1 ± 0.3 μmol h^{-1} at 365 nm and 0.6 ± 0.2 μmol h^{-1} at 415 nm, where the standard deviation is given as the error. One outlier measurement (sample 1, precursor 3) has a lower performance, but the second measurement for the same sample is comparable to all other

results. Without this outlier, the H_2 production rates are 1.3 ± 0.2 μmol h^{-1} and 0.6 ± 0.1 μmol h^{-1} at 365 nm and 415 nm, respectively. These variations may arise from slight differences in the dopant concentrations and/or ratios between batches and samples as well as errors that originate from the photodeposition and PC testing procedure.

Since we have established the promise of FLA treatment in the rapid doping of $SrTiO_3$ powders, it is next worth detailing how the treatment parameters affect the FLA process. The process conditions during FLA are controlled indirectly instead of directly controlling the temperature and time as for conventional TA. Besides the flash parameters (frequency, pulse width, voltage, number of pulses), the light absorption and thermal properties of the material and support are important parameters.[27]

The light absorption properties of the $SrTiO_3$ precursor and Si support differ strongly in our experiments. Si has a band gap of *ca.* 1.1 eV while the band gap of the undoped $SrTiO_3$ precursor is *ca.* 3.2 eV.[57,58] The Si substrate can therefore absorb a much higher fraction of the spectrum of the Xe flash lamp. If a sufficient share of the FLA pulses reaches the substrate, it could thus also show significant photothermal heating and indirectly heat the $SrTiO_3$ powder.

To test if the Si substrate contributes to the heating of the sample during FLA, we compared the FLA of Rh,La-impregnated $SrTiO_3$ powder on Si substrates to non-light absorbing substrates (quartz and Al_2O_3). We found that the loose precursor powder is effectively doped by FLA when deposited on Si while doping is not successful on the non-light absorbing substrates (see sample color on photographs in Fig. 5a and b and S21 for SEM images and Al_2O_3 substrate). We conclude that a crucial contribution to the heating is delivered from the Si substrate to the $SrTiO_3$ precursor through indirect heating. However, we note that likely the light absorption of $SrTiO_3$ and direct photothermal heating of the precursor contributes significantly as well after an initial heating from the substrate. The band gap of $SrTiO_3$ narrows with increasing temperature, thus increasing the absorbed light fraction.[27,58,59] Further, photothermal sintering of $SrTiO_3$ green bodies was reported without using a light absorbing substrate.[27] This suggests that indirect heating from the light-absorbing Si substrate and direct photothermal heating of $SrTiO_3$ both contribute to heat the samples sufficiently for successful Rh,La-doping.

To test the role of the precursor's surface morphology on the effectiveness of the doping process, the FLA doping of the rough commercial precursor was compared to a similar doping process for faceted cubes of undoped $SrTiO_3$ prepared with a hydrothermal synthesis.[60] The particle surface of the rough precursor (incl. undoped references) evolves into a smooth surface during FLA (see SEM images in Fig. 2 and S7 and S8). In contrast, the faceted $SrTiO_3$ cubes do not show significant surface restructuring (see SEM images in Fig. S22a and b). After FLA, the faceted cubes have a brownish color (not the typical yellow color as for the rough precursor, see Fig. 5c and d). STEM-EDX mapping shows well distributed

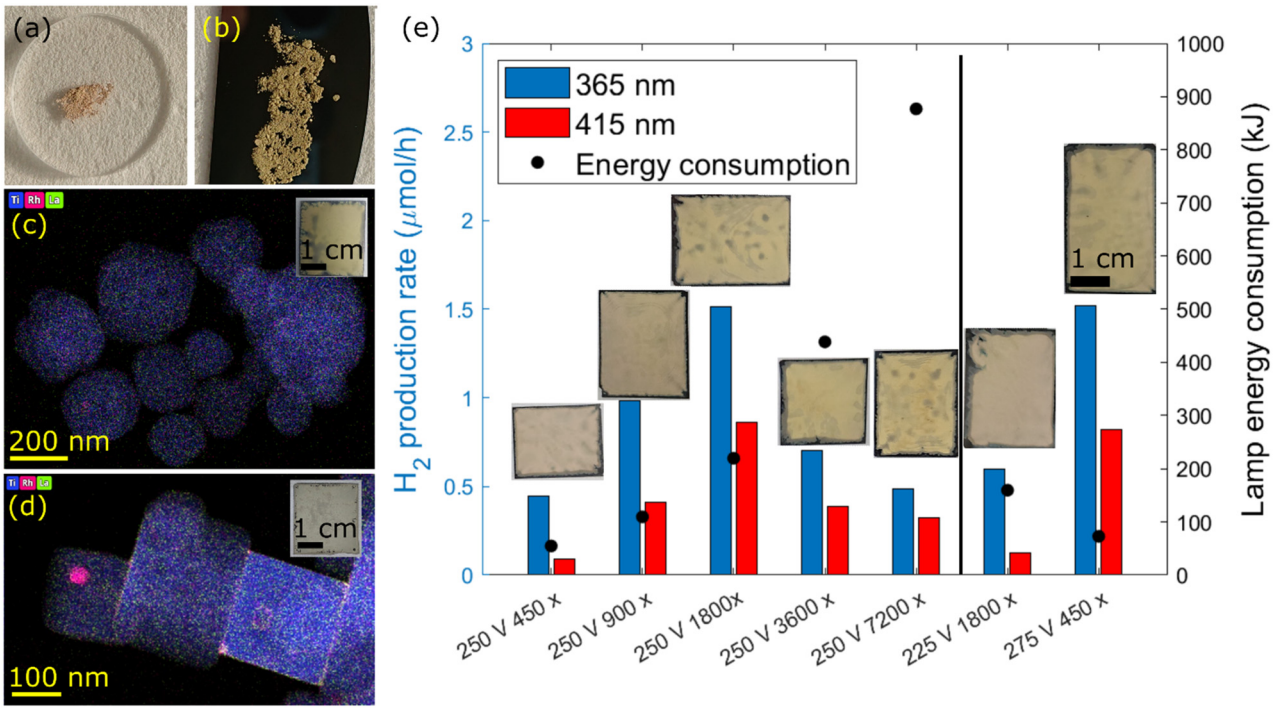

Fig. 5 Photographs after FLA of the Rh,La-impregnated precursor powder at 250 V and 1800 pulses on (a) quartz and (b) Si substrates. STEM-EDX maps and photograph inserts after FLA of Rh,La-impregnated (c) commercial $SrTiO_3$ with rough surface structure and (d) faceted $STiO_3$ cubes. (e) PC performance and photograph inserts of Rh,La:$SrTiO_3$ synthesized with FLA at different process conditions by varying the voltage and number of pulses. The calculated total energy consumption of the flash lamp for each condition is plotted additionally.

dopants when using the rough precursor but strong segregation for the hydrothermal cubes (see Fig. 5c and d). Accordingly, the cubes show no significant PC activity (see Fig. S22c). It is concluded that doping was not successful for the faceted cubes and the restructuring is crucial for rapid dopant incorporation during FLA. Further studies to elucidate the mechanism of dopant incorporation into $SrTiO_3$ precursors are needed to better understand the contribution of diffusion and surface restructuring.

The sensitivity of the H_2 production rate on the variation of the voltage and number of pulses shown in Fig. 5e was used to gain insights on how to control the process temperature and time by these parameters. Varying the number of pulses at 250 V results in a volcano-type evolution of the sample performance starting with only a modest visible light activity when 450 pulses are used, and with an optimum H_2 production rate at 1800 pulses (at which a distinct yellow color is reached, see Fig. S3 for photographs). The performance then decreases continuously with increasing energy input when using 3600 or 7200 pulses. The absorption coefficient in the visible light increases strongly up to 1800 pulses and less significantly afterwards (see Fig. S23). SEM images in Fig. S24 show increasing sintering at 3600 and 7200 pulses. Sufficient heating is thus needed to incorporate the dopants, but prolonged flashing has a similarly detrimental effect on the performance as longer TA. Based on these observations, an initial heating is followed by a regime in which the number of pulses mainly controls the annealing time. FLA therefore gives the opportunity to perform the doping reliably in a time regime not accessible for TA. The reasons for the decreased performance above 1800 pulses can be attributed to a combination of factors including a decreased surface area, changing defect concentrations, and less favorable dopant distributions.

Remaining at 1800 pulses but changing the voltage shows fundamental differences in the occurring process. At 225 V, there is a less pronounced color change and incomplete surface restructuring (see Fig. S3 and S23g for photographs and SEM images, respectively). The visible light performance remains low and doping is thus not completed. At 275 V and 1800 pulses, the Si substrate melted (see photograph and SEM image in Fig. S3 and S24h, respectively). Different temperature regimes are thus reached at different voltages. At 275 V, doping with comparable performance to using 250 V and 1800 pulses is successful after 450 pulses. The process was apparently stopped before reaching a temperature above the melting point of Si, but within the processing window for doping. This condition consumes less total energy than 1800 pulses at 250 V (73.0 kJ *vs.* 219.3, see Table S1 for all energy consumptions). Therefore, optimizing the lamp parameters can also reduce the energy consumption.

The results discussed above promote the view of establishing a thermal equilibrium, which depends on the voltage and the number of pulses (see scheme in Fig. S25). For sintering, the thermal balance of energy input absorbed from the incident light compared to heat losses through convection, IR-emission, and thermal conduction was suggested to allow temperature stabilization.[27] The voltage, frequency, and pulse width control the average power delivered by the lamp, which affects the thermal balance of the sample and thus the established temperature after an initial heating phase. Neither melting of the Si substrate nor the $SrTiO_3$ particles was observed for conditions of successful doping in this work. This suggests that the stabilized temperature for those conditions did not exceed 1414 °C. However, the sample is not illuminated continuously but by 1.5 ms pulses with repetition rate of 60 Hz. The actual temperature reached during the pulse remains unknown since direct temperature measurements are not trivial for these temperature and time scales.[26] The peak temperatures may be significantly higher than the typical processing temperature of 1100 °C. Measurements on the synthesis of single atom catalysts have shown that >2000 °C can be reached in a ms time scale with just one pulse but using a more powerful lamp than in this work.[45] Overall, choosing a suitable support material and lamp parameters can afford control over the FLA process and selection of a suitable processing window for doping of $SrTiO_3$ without exact knowledge of the temperature profile.

On large scale, the energy efficiency of doping *via* FLA compared to TA or other alternative doping processes would be a relevant criterion influencing the final process choice. Qualitatively speaking, FLA and other photothermal techniques differ from conventional TA: photothermal annealing enables targeted heating of just the precursor material while conventional TA requires heating of external equipment (*e.g.* the furnace itself), which also impacts the energy efficiency depending on the batch size. Based on estimated energy demands, Porz *et al.* conclude that light-based sintering processes are significantly more efficient than other available sintering techniques.[27,61] Their study further shows that sintering with blue LEDs needs around 50% less energy than FLA (<2 kWh kg^{-1} *vs.* 4 kWh kg^{-1}).[27] The use of blue LEDs may thus be a more energy-efficient but less mature technique to explore in future studies. To make relevant statements about potential energy savings of doping *via* FLA compared to TA or other methods, the processes should be compared after optimization and considering scale-up effects, which is beyond the scope of this study.

This work established FLA as tunable and reproducible method for the rapid synthesis of core/shell-doped Rh,La:$SrTiO_3$ photocatalysts with superior performance than TA. The comparison to other rapid annealing techniques such as microwave heating, rapid thermal annealing, or laser annealing in future research may provide relevant insight by comparing the effects of different processing methods on the properties of the doped NPs. Further, extending the doping of NPs through FLA to other dopants and materials may be explored in future research.

Conclusions

Flash light annealing (FLA) enables the surface doping of $SrTO_3$ with Rh and La to obtain NPs with an undoped core/doped shell structure within less than 10 s. The restructuring of the rough precursor particle surface is crucial for successful doping by FLA. Doping by FLA incorporates dopants closer to the surface than thermal annealing (TA) and mitigates unwanted particle sintering. The FLA therefore yields Rh,La:$SrTiO_3$ photocatalyst NPs with tripled H_2 evolution compared to conventional TA at 1100 °C for 6 h and 50% improved harvesting of full spectrum illumination compared to the undoped precursor.

The FLA process can be controlled by varying the lamp voltage and number of pulses, which indirectly control the equilibrium temperature and annealing time, respectively. More broadly, this work demonstrates new pathways for the doping of metal oxides within seconds without an ion implantation step and the possibility to process powders instead of thin films or wafers.

Author contributions

M. J. – investigation, methodology, writing – original draft, conceptualization; W. O. S. – methodology, investigation, writing – review & editing; A. D. – software, methodology, writing – original draft; P. K. – software, methodology, writing – original draft; M. B. – investigation; A. B. – investigation; C. F. G. – supervision; H. J. – supervision; R. D. – funding acquisition; M. S. – funding acquisition, methodology, resources, writing – review & editing; K. S. – funding acquisition, resources, conceptualization, writing – review & editing. All co-authors have read and agreed to the final version of the manuscript.

Conflicts of interest

There are no conflicts to declare.

Data availability

The data that support the findings of this study are available from the corresponding author upon reasonable request.

Supplementary information (SI): experimental details and supporting experiments and characterization. See DOI: https://doi.org/10.1039/d5cy01501d.

Acknowledgements

The research was financially supported by Toyota Motor Europe, Brussels, Belgium. The authors (AD, RDI) acknowledge funding by the Federal Ministry of Research, Technology and Space (BMFTR) under grant No. 03SF0757. All authors acknowledge the assistance of Mounir Mensi for conducting and analyzing the XPS measurements and David Reyes Vasquez with CBED and HRTEM imaging. ICP-MS was performed at the Central Environmental Laboratory (GR-CEL) of EPFL. The temporary support of Alexandre Fulconis with the conduction of flash light annealing was highly appreciated.

Notes and references

1 B. A. Pinaud, J. D. Benck, L. C. Seitz, A. J. Forman, Z. Chen, T. G. Deutsch, B. D. James, K. N. Baum, G. N. Baum, S. Ardo, H. Wang, E. Miller and T. F. Jaramillo, *Energy Environ. Sci.*, 2013, **6**, 1983.
2 J. Hyun Kim, D. Hansora, P. Sharma, J.-W. Jang and J. Sung Lee, *Chem. Soc. Rev.*, 2019, **48**, 1908–1971.
3 P. Zhou, I. A. Navid, Y. Ma, Y. Xiao, P. Wang, Z. Ye, B. Zhou, K. Sun and Z. Mi, *Nature*, 2023, **613**, 66–70.
4 Y. Li, Y.-K. Peng, L. Hu, J. Zheng, D. Prabhakaran, S. Wu, T. J. Puchtler, M. Li, K.-Y. Wong, R. A. Taylor and S. C. E. Tsang, *Nat. Commun.*, 2019, **10**, 4421.
5 Q. Wang, T. Hisatomi, Q. Jia, H. Tokudome, M. Zhong, C. Wang, Z. Pan, T. Takata, M. Nakabayashi, N. Shibata, Y. Li, I. D. Sharp, A. Kudo, T. Yamada and K. Domen, *Nat. Mater.*, 2016, **15**, 611–615.
6 Z. Pan, J. J. M. Vequizo, H. Yoshida, J. Li, X. Zheng, C. Chu, Q. Wang, M. Cai, S. Sun, K. Katayama, A. Yamakata and K. Domen, *Angew. Chem.*, 2025, **137**, e202414628.
7 H. Fu, Y. Wu, Y. Guo, T. Sakurai, Q. Zhang, Y. Liu, Z. Zheng, H. Cheng, Z. Wang, B. Huang, Q. Wang, K. Domen and P. Wang, *Nat. Commun.*, 2025, **16**, 990.
8 C. Avcıoğlu, S. Avcıoğlu, M. F. Bekheet and A. Gurlo, *ACS Appl. Energy Mater.*, 2023, **6**, 1134–1154.
9 T. Takata, J. Jiang, Y. Sakata, M. Nakabayashi, N. Shibata, V. Nandal, K. Seki, T. Hisatomi and K. Domen, *Nature*, 2020, **581**, 411–414.
10 H. Lyu, T. Hisatomi, Y. Goto, M. Yoshida, T. Higashi, M. Katayama, T. Takata, T. Minegishi, H. Nishiyama, T. Yamada, Y. Sakata, K. Asakura and K. Domen, *Chem. Sci.*, 2019, **10**, 3196–3201.
11 H. Nishiyama, T. Yamada, M. Nakabayashi, Y. Maehara, M. Yamaguchi, Y. Kuromiya, Y. Nagatsuma, H. Tokudome, S. Akiyama, T. Watanabe, R. Narushima, S. Okunaka, N. Shibata, T. Takata, T. Hisatomi and K. Domen, *Nature*, 2021, **598**, 304–307.
12 Q. Wang, T. Hisatomi, S. S. K. Ma, Y. Li and K. Domen, *Chem. Mater.*, 2014, **26**, 4144–4150.
13 R. Han, M. A. Jr, Z. Melo, Z. Wu Zhao and F. E. Osterloh, *J. Phys. Chem. C*, 2020, **124**, 9724–9733.
14 M. A. Melo Jr., Z. Wu, B. A. Nail, A. T. De Denko, A. F. Nogueira and F. E. Osterloh, *Nano Lett.*, 2018, **18**, 805–810.
15 X. Li, H. Zhao, J. Liang, Y. Luo, G. Chen, X. Shi, S. Lu, S. Gao, J. Hu, Q. Liu and X. Sun, *J. Mater. Chem. A*, 2021, **9**, 6650–6670.
16 R. Konta, T. Ishii, H. Kato and A. Kudo, *J. Phys. Chem. B*, 2004, **108**, 8992–8995.
17 R. Asai, H. Nemoto, Q. Jia, K. Saito, A. Iwase and A. Kudo, *Chem. Commun.*, 2014, **50**, 2543–2546.
18 R. Niishiro, S. Tanaka and A. Kudo, *Appl. Catal., B*, 2014, **150–151**, 187–196.

19 B. Moss, Q. Wang, K. T. Butler, R. Grau-Crespo, S. Selim, A. Regoutz, T. Hisatomi, R. Godin, D. J. Payne, A. Kafizas, K. Domen, L. Steier and J. R. Durrant, *Nat. Mater.*, 2021, **20**, 511–517.
20 D. H. K. Murthy, H. Matsuzaki, Q. Wang, Y. Suzuki, K. Seki, T. Hisatomi, T. Yamada, A. Kudo, K. Domen and A. Furube, *Sustainable Energy Fuels*, 2019, **3**, 208–218.
21 L. An, M. Kitta, A. Iwase, A. Kudo, N. Ichikuni and H. Onishi, *ACS Catal.*, 2018, **8**, 9334–9341.
22 H. Sudrajat, M. Kitta, R. Ito, T. Yoshida, R. Katoh, B. Ohtani, N. Ichikuni and H. Onishi, *Phys. Chem. Chem. Phys.*, 2021, **23**, 8868–8879.
23 H. Sudrajat, D. Dhakal, M. Kitta, T. Sasaki, A. Ozawa, S. Babel, T. Yoshida, N. Ichikuni and H. Onishi, *J. Phys. Chem. C*, 2019, **123**, 18387–18397.
24 N.-H. Park, F. Dang, C. Wan, W.-S. Seo and K. Koumoto, *J. Asian Ceram. Soc.*, 2013, **1**, 35–40.
25 Y. Fan, G. Zhang, H. Zhou, Y. Qiu, W. Wang and F. Dang, *Adv. Compos. Hybrid Mater.*, 2023, **6**, 209.
26 L. Rebohle, S. Prucnal and W. Skorupa, *Semicond. Sci. Technol.*, 2016, **31**, 103001.
27 L. Porz, M. Scherer, D. Huhn, L.-M. Heine, S. Britten, L. Rebohle, M. Neubert, M. Brown, P. Lascelles, R. Kitson, D. Rettenwander, L. Fulanovic, E. Bruder, P. Breckner, D. Isaia, T. Frömling, J. Rödel and W. Rheinheimer, *Mater. Horiz.*, 2022, **9**, 1717–1726.
28 L. Rebohle, S. Prucnal and D. Reichel, *Flash Lamp Annealing: From Basics to Applications*, Springer International Publishing, Cham, 2019, vol. 288.
29 R. Abbel, T. van Lammeren, R. Hendriks, J. Ploegmakers, E. J. Rubingh, E. R. Meinders and W. A. Groen, *MRS Commun.*, 2012, **2**, 145–150.
30 S. Prucnal, L. Rebohle and W. Skorupa, *Mater. Sci. Semicond. Process.*, 2017, 115–127.
31 *Subsecond Annealing of Advanced Materials: Annealing by Lasers, Flash Lamps and Swift Heavy Ions*, ed. W. Skorupa and H. Schmidt, Springer International Publishing, Cham, 2014, vol. 192.
32 P. Timans, J. Gelpey, S. McCoy, W. Lerch and S. Paul, *MRS Online Proc. Libr.*, 2006, **912**, 101.
33 K. Nishiyama, M. Arai and N. Watanabe, *Jpn. J. Appl. Phys.*, 1980, **19**, L563–L566.
34 J. Troughton, C. Charbonneau, M. J. Carnie, M. L. Davies, D. A. Worsley and T. M. Watson, *J. Mater. Chem. A*, 2015, **3**, 9123–9127.
35 S. Sanchez, X. Hua, N. Phung, U. Steiner and A. Abate, *Adv. Energy Mater.*, 2018, **8**, 1702915.
36 M. Scherer, M.-G. Ameres, W. Rheinheimer, T. Frömling, J. Rödel and L. Fulanović, *J. Eur. Ceram. Soc.*, 2023, **43**, 5406–5411.
37 L. Porz, M. Scherer, Q. K. Muhammad, K. Higuchi, Y. Li, S. Koga, A. Nakamura, W. Rheinheimer and T. Frömling, *J. Am. Ceram. Soc.*, 2022, **105**, 7030–7035.
38 B. Yoon, D. Yadav, S. Ghose and R. Raj, *J. Am. Ceram. Soc.*, 2019, **102**, 2294–2303.
39 T. Ito, T. Iinuma, A. Murakoshi, H. Akutsu, K. Suguro, T. Arikado, K. Okumura, M. Yoshioka, T. Owada, Y. Imaoka, H. Murayama and T. Kusuda, in *Extended Abstracts of the 2001 International Conference on Solid State Devices and Materials*, Tokyo, Japan, 2001, vol. A-5-3, pp. 182–183.
40 J.-S. Park, D.-J. Kim, W.-H. Chung, Y. Lim, H.-S. Kim and Y.-B. Kim, *Sci. Rep.*, 2017, **7**, 12458.
41 J.-S. Park, W.-H. Chung, H.-S. Kim and Y.-B. Kim, *J. Alloys Compd.*, 2017, **696**, 102–108.
42 A. Lesch, *Adv. Mater. Technol.*, 2018, **3**, 1700201.
43 V. Costa Bassetto, M. Mensi, E. Oveisi, H. H. Girault and A. Lesch, *ACS Appl. Energy Mater.*, 2019, **2**, 6322–6331.
44 W. O. Silva, A. Mabillard, M. Soutrenon, G. Gschwend, Y. Ligen, S. Joris, L. Bondaz, K. V. Agrawal and H. H. Girault, *J. Mater. Chem. A*, 2025, **13**, 7403–7412.
45 D.-H. Kim, J.-H. Cha, S. Chong, S.-H. Cho, H. Shin, J. Ahn, D. Jeon, J. Kim, S.-Y. Choi and I.-D. Kim, *ACS Nano*, 2023, **17**, 23347–23358.
46 H. Gong, Z. Gong, J. Liu, G. Ye and H. Fei, *Adv. Funct. Mater.*, 2024, **34**, 2316438.
47 K. Wiesenhütter and W. Skorupa, in *Subsecond Annealing of Advanced Materials: Annealing by Lasers, Flash Lamps and Swift Heavy Ions*, ed. W. Skorupa and H. Schmidt, Springer International Publishing, Cham, 2014, pp. 271–295.
48 P. Kant, phoRex & QY photoreactor - Monte Carlo ray tracing in MATLAB® & quantum yield measurements, https://publikationen.bibliothek.kit.edu/1000150817, (accessed 20 August 2025).
49 P. Kant, L. L. Trinkies, N. Gensior, D. Fischer, M. Rubin, G. Alan Ozin and R. Dittmeyer, *Chem. Eng. J.*, 2023, **452**, 139204.
50 P. P. Kant, Optimierung von Fotokatalysatoren und Fotoreaktoren für die Synthese solarer Kraftstoffe = Optimizing photocatalysts and photoreactors for solar fuel synthesis, https://publikationen.bibliothek.kit.edu/1000162170, (accessed 20 August 2025).
51 H. C. Hulst and H. C. van de Hulst, *Light Scattering by Small Particles*, Courier Corporation, 1981.
52 B. Modak and S. K. Ghosh, *J. Phys. Chem. B*, 2015, **119**, 11089–11098.
53 K. Szot, W. Speier, U. Breuer, R. Meyer, J. Szade and R. Waser, *Surf. Sci.*, 2000, **460**, 112–128.
54 H. Wei, W. Maus-Friedrichs, G. Lilienkamp, V. Kempter, J. Helmbold, K. Gömann and G. Borchardt, *J. Electroceram.*, 2002, **8**, 221–228.
55 H. Wei, L. Beuermann, J. Helmbold, G. Borchardt, V. Kempter, G. Lilienkamp and W. Maus-Friedrichs, *J. Eur. Ceram. Soc.*, 2001, **21**, 1677–1680.
56 T. D. Small, M. A. Hamza, Y. Shen, C. J. Shearer and G. F. Metha, *Nanoscale Adv.*, 2025, **7**, 4313–4324.
57 W. Bludau, A. Onton and W. Heinke, *J. Appl. Phys.*, 1974, **45**, 1846–1848.
58 D. J. Kok, K. Irmscher, M. Naumann, C. Guguschev, Z. Galazka and R. Uecker, *Phys. Status Solidi A*, 2015, **212**, 1880–1887.
59 T. Bieger, J. Maier and R. Waser, *Solid State Ionics*, 1992, **53–56**, 578–582.

60 L. Mu, Y. Zhao, A. Li, S. Wang, Z. Wang, J. Yang, Y. Wang, T. Liu, R. Chen, J. Zhu, F. Fan, R. Li and C. Li, *Energy Environ. Sci.*, 2016, **9**, 2463–2469.

61 T. Ibn-Mohammed, C. A. Randall, K. B. Mustapha, J. Guo, J. Walker, S. Berbano, S. C. L. Koh, D. Wang, D. C. Sinclair and I. M. Reaney, *J. Eur. Ceram. Soc.*, 2019, **39**, 5213–5235.